Spontaneous Exciton Valley Coherence in Transition Metal Dichalcogenide Monolayers Interfaced with an Anisotropic Metasurface

Pankaj K. Jha, Nir Shitrit, Xuexin Ren, Yuan Wang, and Xiang Zhang

Phys. Rev. Lett. **121**, 116102 — Published 11 September 2018

DOI: 10.1103/PhysRevLett.121.116102

Spontaneous Exciton Valley Coherence in Transition Metal Dichalcogenide Monolayers Interfaced with an Anisotropic Metasurface

Pankaj K. Jha[1†], Nir Shitrit[1†], Xuexin Ren[1], Yuan Wang[1], and Xiang Zhang[1,2*]

[1]*NSF Nanoscale Science and Engineering Center (NSEC),*

3112 Etcheverry Hall, University of California, Berkeley, California 94720, USA

[2]*Materials Sciences Division, Lawrence Berkeley National Laboratory,*

1 Cyclotron Road, Berkeley, California 94720, USA

(Dated: August 14, 2018)

[†]These authors contributed equally to this work.

[*]E-mail: xiang@berkeley.edu

Abstract

The control of the exciton intervalley coherence renders transition metal dichalcogenides monolayers promising candidates for quantum information science. So far, generating intervalley coherence has the need for an external coherent field. Here, we theoretically demonstrate spontaneous generation (i.e., without any external field) of exciton intervalley coherence. We achieve this by manipulating the vacuum field in the vicinity of the monolayer with a designed polarization-dependent metasurface, inducing an anisotropic decay rate for in-plane excitonic dipoles. Harnessing quantum coherence and interference effects in two-dimensional materials may provide the route for novel quantum valleytronic devices.

Coherent superposition of states (i.e., quantum coherence) is a fundamental feature of quantum mechanics marking its departure from the classical realm [1]. For elementary particles, such as atoms, ions and photons, quantum coherence is an essential ingredient for a plethora of phenomena in quantum optics [2], quantum information science [3] and condensed matter physics [4]. In semiconductors, excitons (Coulomb-bound electron-hole pairs), which are the fundamental quasiparticles, also exhibit coherence. Excitonic coherence plays a crucial role in quantum dots [5], quantum-well structures [6] and light-harvesting complexes [7]. Recently, atomically thin transition metal dichalcogenides (TMDCs) of the form MX_2 (M=Mo, W; X=S, Se, Te) have emerged as a new class of semiconductor materials for both fundamental physics exploration in two-dimensional systems and device applications [8-10]. These monolayer semiconductors are manifested by a direct bandgap between the extrema of valence and conduction bands residing at the energy-degenerate K and K′ points of the Brillouin zone. Owing to the broken inversion symmetry in monolayer TMDCs, excitons exhibit valley-dependent optical selection rule [11,12]. More specifically, excitons in the K and K′ valleys are coupled to photons with the same energy but mutually-orthogonal polarization helicities $\sigma_{\pm}$, respectively.

Harnessing the valley degree of freedom in TMDC monolayers for quantum information processing requires coherent manipulation of excitons in the K and K′ valleys, in addition to the inherent selective excitation. The coherence among the valleys (optical alignment of excitons), i.e., valley coherence, was revealed by the observation of a linearly polarized emission (coherent superposition of $\sigma_{\pm}$ photons) from a TMDC monolayer optically excited by a linearly polarized light [13]. However, all previous approaches to generate valley coherence require the presence of an external coherent field [13-19]. In this letter, we theoretically demonstrate that intervalley coherence can be *spontaneously* generated in TMDC monolayers *without* any external field. We achieve this neutral exciton intervalley coherence by manipulating the vacuum field in the vicinity of the TMDC monolayer with a designed light molding interface (metasurface), exhibiting in-plane polarization-dependent response. Note that the optical selection rule [11,12] forbids such a vacuum-induced coherence among mutually orthogonal K and K′ valleys in free space. The spontaneous exciton valley coherence in TMDC monolayers opens a new paradigm in two-dimensional materials exploiting quantum interference effects for optoelectronic applications [10,20] and novel valleytronic devices [21].

We considered an atomically thin layer (monolayer) of TMDC of type MX_2 interfaced with a two-dimensional array of subwavelength-spaced optical nanoantenna phase shifters – a metasurface (Fig. 1). Photonic metasurfaces enable a custom-tailored electromagnetic response with unprecedented control over the fundamental properties of light, i.e., phase, amplitude, and polarization [22-24]. We assumed that initially one electron is excited to the lowest level of the conduction band of K valley ($|c_{\mathrm{K}}\rangle$). In free space, which is a homogeneous, isotropic and linear medium, this excited electron returns to the ground state (i.e., highest level of the valence band $|v_{\mathrm{K}}\rangle$) by emitting a photon with an energy corresponding to the $|c_{\mathrm{K}}\rangle \leftrightarrow |v_{\mathrm{K}}\rangle$ transition. The transient response of the population is $e^{-\gamma_{\mathrm{K}} t}$ and the emission cannot excite the orthogonal K′ valley electron. However, by breaking the isotropic nature of the quantum vacuum [25] in the vicinity of the TMDC monolayer, the emission from K valley can radiatively excite the electron in K′ valley and vice versa.

The electron-hole pair at the valleys of the TMDC monolayer can be treated as a local in-plane excitonic dipole. The interaction between such a quantum emitter and its spontaneous emission that is molded by the metasurface is dictated by the dipole scattered field, i.e., a secondary field of the dipole that was emitted and then probed at a target position after it was scattered in the environment. For calculating the scattered field, we used the method of dipole-metasurface interaction [26]. For achieving an anisotropic quantum vacuum, we designed the metasurface such that it imprints opposite phase profiles to the projected circular polarization states of the incident field $\mathbf{E}(z=0^+,\mathbf{r},\omega)$, where $\mathbf{r}=(x,y,0)$ is the vector position at the metasurface plane, and ω is the atomic $|c_{\mathrm{K}}\rangle \leftrightarrow |v_{\mathrm{K}}\rangle$ transition frequency. Subsequently, we expressed the transverse x and y components of the reflected field just above the metasurface as

$$\mathbf{E}_r(z=0^+,\mathbf{r},\omega) = -\sqrt{\eta}\mathbf{U}^{-1}\begin{pmatrix} 0 & e^{-i\Phi(x,y)} \\ e^{i\Phi(x,y)} & 0 \end{pmatrix}\mathbf{U}\mathbf{E}(z=0^+,\mathbf{r},\omega). \qquad (1)$$

Here, η is the cross-polarization reflectivity of the metasurface, $\mathbf{U}=\frac{1}{\sqrt{2}}\begin{pmatrix}1 & i\\ 1 & -i\end{pmatrix}$ is a unitary conversion matrix transforming from Cartesian basis to helicity basis, and $\Phi(x,y)$ is the imprinted phase profile for right-handed circularly polarized light. The off-diagonal matrix represents the interaction of circularly polarized light with the metasurface, where the off-diagonal terms are associated with the flipping of the circular polarizations by the metasurface. Finally, by employing the Huygens-Fresnel diffraction integral, the scattered field at the desired point is calculated [26].

We engineer an anisotropic quantum vacuum by introducing a designed interface that its role is to refocus the emitted light from the excitonic dipole to itself for both x and y polarizations of the dipole; however, the scattered field at the location of the dipole for these polarizations reverses sign (i.e., π-phase shifted). Such a polarization-dependent response of the metasurface gives rise to an anisotropic decay rate, in which for one polarization of the dipole, the decay rate is enhanced while for the second polarization, the decay rate is symmetrically suppressed. The light bending by the metasurface of all light paths from source to interface and from interface to source [see Fig. 3(a)] is optically equivalent to compensation of the phase accumulated via propagation through free space by the phase shift imparted by the metasurface. The required anisotropic response was realized by a geometric phase-based metasurface (GPM), wherein the polarization helicity is a degree of freedom. The pickup of the geometric Pancharatnam-Berry phase [27,28] in metasurfaces arises from space-variant manipulation of the polarization state of light, enabled by tilling a surface with anisotropic nanoantennas arranged according to an on-demand space-variant orientation angle profile $\theta(x,y)$ [22,29-33]. A GPM converts an incident circularly polarized light into a beam of opposite circular polarization, imprinted with a geometric phase $\Phi(x,y) = 2\sigma_{\pm}\theta(x,y)$, where $\sigma_{\pm} = \pm 1$ is the polarization helicity of the incident light corresponding to right and left circularly polarized light, respectively [22,29-33]. Here, we imprint opposite phase profiles to the projected circular polarization states of the incident field via a GPM to achieve the prescribed anisotropic quantum vacuum. We consider the position of the excitonic dipole at $(0,0,d)$, where d is the distance between the quantum emitter and the metasurface [see Fig. 3(a)]. Accordingly, the phase profile imprinted at the metasurface is $\Phi(x,y) = -2k\sigma_{\pm}\left(\sqrt{x^2 + y^2 + d^2} - \pi\right)$, where x and y are the metasurface coordinates, $k = 2\pi/\lambda$ is the wavenumber, and λ is the wavelength corresponding to the $|c_{\mathrm{K}}\rangle \leftrightarrow |v_{\mathrm{K}}\rangle$ atomic transition. We realized this phase profile by locally orienting the antennas according to the space-variant angle profile $\theta(x,y) = \Phi(x,y)/2\sigma_{\pm}$ [Figs. 2(a) and 2(b)]. The individual antenna is a gap plasmon resonator nanoantenna consisting of metal-insulator-metal layers enabling high reflectivity by increasing the coupling between the free wave and the fundamental resonator mode [34]. We designed the dimensions of the nanoantenna to locally mimic a half-wave plate for the reflected light, yielding highly efficient GPMs [32,35]. For the wavelength of 670 nm, which is the resonant wavelength for molybdenum disulfide (MoS_2) monolayer, we achieved 90% cross-polarization reflectivity for the components flipping the polarization helicity

of the incident wave, whereas the co-polarization reflectivity for the components maintaining the polarization is extremely low (~0.1%) [Fig. 2(c)] (see Supplemental Material [36], Sec. 1 for the calculation of the cross-polarization and co-polarization reflectivities). Note that these reflectivities are robust over a large bandwidth of ~200 nm [Fig. 2(c)].

By applying the method of dipole-metasurface interaction [26], we obtained the distribution of the scattered field intensity for x- or y-polarized source dipoles, where the efficient light focused back via the metasurface to the quantum emitter is evident [Fig. 3(a)]. We also calculated the imaginary part of the scattered field at varying x positions to reveal that the metasurface-governed scattered field at the position of the dipole is minimized for a x-polarized dipole while symmetrically maximized for a y-polarized dipole [Fig. 3(b)]. Note that we designed the phase profile of the metasurface such that the imaginary part of the scattered field is predominant while the real part is suppressed. By considering a finite size metasurface, the ohmic loss due to the metal and the phase discretization loss [37], we achieved that ~47% of the dipole source field emission is focused back to the dipole. Such a polarization-dependent scattered field $\mathbf{E}_s$ results in an engineered anisotropic decay rate γ of the quantum emitter as [38]

$$\frac{\gamma(\mathbf{r}_1)}{\gamma_0} = 1 + \frac{6\pi\varepsilon_0}{|\boldsymbol{\wp}|^2}\frac{1}{k^3}\mathrm{Im}[\boldsymbol{\wp}^* \cdot \mathbf{E}_s(\mathbf{r}_1,\mathbf{r}_1,\omega)]. \quad (2)$$

Here, γ_0 is the vacuum spontaneous emission decay rate, $\mathbf{r}_1$ is the position vector of the dipole, ε_0 is the vacuum permittivity, and $\boldsymbol{\wp}$ is the transition dipole moment of the excitonic dipole. Therefore, the reversed sign of the scattered field at the location of the dipole for x- and y-polarized dipoles [Fig. 3(b)] gives rise to an anisotropic quantum vacuum, where the engineered normalized decay rate is suppressed (0.53) and symmetrically enhanced (1.47) for x- and y-polarized dipoles, respectively [Fig. 3(c)]. Note that in the ideal limit of a lossless and infinitely large GPM, the change in the normalized decay rate is 0.5 [see red and blue lines in Fig. 3(c)] (see Supplemental Material [36], Secs. 2 and 3 for the wavelength- and distance-dependent responses of the metasurface-enabled anisotropic decay rate, respectively, and Sec. 4 for the effect of the metasurface size on the engineered decay rate).

The interaction between the quantum vacuum field (i.e., quantum state with the lowest possible energy in the absence of excitations) and the exciton in the TMDC monolayer gives rise to the emergence of intervalley coherence. In the interaction picture, the density operator $\varrho(t)$ of the combined exciton-field system satisfies the Liouville-von Neumann equation [39]

$$\frac{\partial \varrho}{\partial t} = -\frac{i}{\hbar}[\mathcal{H}, \varrho] - \mathcal{L}\varrho. \quad (3)$$

Here, $\mathcal{L}$ is the Lindblad superoperator quantifying the relaxation (radiative and nonradiative) and fluctuations in an excitonic system, $\mathcal{H}$ is the interaction Hamiltonian corresponding to the coupling of the degenerate valley (K and K′) with the vacuum field, and $\hbar$ is the reduced Planck's constant. In the excitation picture, the excitons at K and K′ can be modelled as a three-level V-system (see Fig. 1 left inset) [16]. The exciton population decay rate in the K and K′ valleys is given by $\gamma_{\mathrm{K/K'}} = \gamma^{r}_{\mathrm{K/K'}} + \gamma^{nr}_{\mathrm{K/K'}}$ (radiative and nonradiative decay rates), and the exciton valley coherence corresponds to the coherent superposition of excitons in K and K′ valleys. The lifetime of the valley coherence is determined by radiative and nonradiative decay rates and the intervalley scattering rate γ_s. Recently, near-unity quantum yield in MoS_2 has been experimentally demonstrated [40,41]; hence, we can assume that $\gamma_{\mathrm{K/K'}} \approx \gamma^{r}_{\mathrm{K/K'}}$. An optical selection rule forbids the excitation of K′ valley exciton with σ_+ polarized light, thus enabling nearly unity valley polarization in monolayers of TMDCs. However, by manipulating the vacuum in the vicinity of the exciton, one can radiatively excite K′ exciton using emission from K valley exciton, and remarkably induce coherence *without* external coherent source.

We consider an exciton in the lowest energy of the valley K initially prepared by resonant optical excitation. From Eq. (3), using the standard projection operator method [42], we obtained the excitonic density matrix element $\langle c_{\mathrm{K'}}|\varrho|c_{\mathrm{K}}\rangle$, that represents the exciton intervalley coherence, at $t \approx 0$ as

$$\frac{\partial}{\partial t}\langle c_{\mathrm{K'}}|\varrho|c_{\mathrm{K}}\rangle = -\frac{1}{2}(\kappa + i\Omega). \quad (4)$$

Here κ and Ω are the vacuum field mediated coupling and frequency shift, respectively, associated with the imaginary and real parts of the scattered field, respectively (see Supplemental Material [36], Sec. 5 for the detailed analysis). Note that we designed the phase profile of the metasurface such that the imaginary part of the scattered field is enhanced while the real part is suppressed, giving rise to predominant κ ($-1 \leq \kappa \leq 1$) and negligible Ω ($\Omega \approx 0$). Equation (4) implies that only in the presence of the vacuum field mediated parameters, nonzero exciton valley coherence emerges. For a circularly-polarized dipole, the coupling term is given by $\kappa = (\gamma_{xx} - \gamma_{yy})/2$, where γ_{xx} (γ_{yy}) represents the decay rate of a dipole oriented along the x (y) axis. For $\kappa \neq 0$, we need $\gamma_{xx} \neq \gamma_{yy}$, i.e., a structured environment, where different in-plane dipoles decay at different rates. We designed a metasurface which breaks the in-plane isotropic

nature of the vacuum at the location of the exciton such that the emission rate for a x-polarized dipole is suppressed while the decay rate for a y-polarized dipole is symmetrically enhanced. Note that such an engineered anisotropic vacuum increases the contrast between the in-plane decay rates, enabling to maximize the vacuum field mediated coupling. Taking into account all loss channels, we obtained $\gamma_{xx} = 0.53$ and $\gamma_{yy} = 1.47$, which yields $\kappa = -0.47$. Figure 4(a) shows the population of excitons in the K and K′ valleys, given by the excitonic density matrix elements $\langle c_{\mathrm{K}}|\varrho|c_{\mathrm{K}}\rangle$ and $\langle c_{\mathrm{K}'}|\varrho|c_{\mathrm{K}'}\rangle$, respectively. In free space, the K valley exciton decays exponentially (dashed line) with a rate $\gamma_{\mathrm{K}} \approx \gamma_{\mathrm{K}}^{r}$ and the K′ valley exciton is not excited (due to a selection rule). However, in the presence of a metasurface, the decay rate of K valley exciton slows down and a finite generation of K′ valley exciton is clearly seen. Figure 4(b) shows the temporal evolution of the exciton valley coherence. In the presence of a metasurface, a finite exciton valley coherence emerges that reaches its maximum value of ~0.09, and then dies gradually. However, in free space (or any other interface that does not break the in-plane isotropic response, e.g., a mirror), $\kappa = \Omega = 0$ and thus, excitonic valley coherence does not emerge and remains zero, as shown by the dashed line in Fig. 4(b). Moreover, this spontaneously generated intervalley coherence survives in the presence of dominant intervalley scattering, even when it is 1000-fold stronger than the spontaneous decay rate [Fig. 4(b) inset].

In summary, we reported on a spontaneous generation of intervalley coherence in TMDCs by interfacing a metasurface with a MoS_2 monolayer. Although we considered the MoS_2 monolayer, this proposal is general and can be implemented in different two-dimensional material systems. The metasurface-enabled unprecedented control over the polarization of light gives rise to an anisotropic quantum vacuum in the vicinity of the TMDC monolayer. While intervalley coherence via a vacuum field mediated coupling is forbidden in free space, metasurfaces offer a route to lift the degeneracy in the optical response of in-plane exitonic dipoles. The reported concept of metaphotonics-enabled quantum coherence and interference effects [26,43-46] in TMDC monolayers may pave the way for the integration of designer metasurfaces with two-dimensional materials [47-50] for quantum valleytronic metadevices.

References

[1] A. Streltsov, G. Adesso, and M. B. Plenio, *Colloquium: Quantum Coherence as a Resource*, Rev. Mod. Phys. **89**, 041003 (2017).

[2] L. Mandel and E. Wolf, *Optical Coherence and Quantum Optics* (Cambridge University Press, Cambridge, 1995).

[3] H. J. Kimble, *The Quantum Internet*, Nature **453**, 1023 (2008).

[4] R. Hanson and D. D. Awschalom, *Coherent Manipulation of Single Spins in Semiconductors*, Nature **453**, 1043 (2008).

[5] W. W. Chow, H. C. Schneider, and M. C. Phillips, *Theory of Quantum-Coherence Phenomena in Semiconductor Quantum Dots*, Phys. Rev. A **68**, 053802 (2003).

[6] G. B. Serapiglia, E. Paspalakis, C. Sirtori, K. L. Vodopyanov, and C. C. Phillips, *Laser-Induced Quantum Coherence in a Semiconductor Quantum Well*, Phys. Rev. Lett. **84**, 1019 (2000).

[7] G. S. Engel, T. R. Calhoun, E. L. Read, T.-K. Ahn, T. Mančal, Y.-C. Cheng, R. E. Blankenship, and G. R. Fleming, *Evidence for Wavelike Energy Transfer through Quantum Coherence in Photosynthetic Systems*, Nature **446**, 782 (2007).

[8] K. F. Mak, C. Lee, J. Hone, J. Shan, and T. F. Heinz, *Atomically Thin MoS_2: A New Direct-Gap Semiconductor*, Phys. Rev. Lett. **105**, 136805 (2010).

[9] Q. H. Wang, K. Kalantar-Zadeh, A. Kis, J. N. Coleman, and M. S. Strano, *Electronics and Optoelectronics of Two-Dimensional Transition Metal Dichalcogenides*, Nat. Nanotechnol. **7**, 699 (2012).

[10] Z. Ye, T. Cao, K. O'Brien, H. Zhu, X. Yin, Y. Wang, S. G. Louie, and X. Zhang, *Probing Excitonic Dark States in Single-Layer Tungsten Disulphide*, Nature **513**, 214 (2014).

[11] H. Zeng, J. Dai, W. Yao, D. Xiao, and X. Cui, *Valley Polarization in MoS_2 Monolayers by Optical Pumping*, Nat. Nanotechnol. **7**, 490 (2012).

[12] K. F. Mak, K. He, J. Shan, and T. F. Heinz, *Control of Valley Polarization in Monolayer MoS_2 by Optical Helicity*, Nat. Nanotechnol. **7**, 494 (2012).

[13] A. M. Jones, H. Yu, N. J. Ghimire, S. Wu, G. Aivazian, J. S. Ross, B. Zhao, J. Yan, D. G. Mandrus, D. Xiao *et al.*, *Optical Generation of Excitonic Valley Coherence in Monolayer WSe_2*, Nat. Nanotechnol. **8**, 634 (2013).

[14] C. R. Zhu, K. Zhang, M. Glazov, B. Urbaszek, T. Amand, Z. W. Ji, B. L. Liu, and X. Marie, *Exciton Valley Dynamics Probed by Kerr Rotation in WSe_2 Monolayers*, Phys. Rev. B **90**, 161302 (2014).

[15] M. Tokman, Y. Wang, and A. Belyanin, *Valley Entanglement of Excitons in Monolayers of Transition-Metal Dichalcogenides*, Phys. Rev. B **92**, 075409 (2015).

[16] K. Hao, G. Moody, F. Wu, C. K. Dass, L. Xu, C.-H. Chen, L. Sun, M.-Y. Li, L.-J. Li, A. H. MacDonald *et al.*, *Direct Measurement of Exciton Valley Coherence in Monolayer WSe_2*, Nat. Phys. **12**, 677 (2016).

[17] R. Schmidt, A. Arora, G. Plechinger, P. Nagler, A. Granados del Águila, M. V. Ballottin, P. C. M. Christianen, S. Michaelis de Vasconcellos, C. Schüller, T. Korn *et al.*, *Magnetic-Field-Induced Rotation of Polarized Light Emission from Monolayer WS_2*, Phys. Rev. Lett. **117**, 077402 (2016).

[18] G. Wang, X. Marie, B. L. Liu, T. Amand, C. Robert, F. Cadiz, P. Renucci, and B. Urbaszek, *Control of Exciton Valley Coherence in Transition Metal Dichalcogenide Monolayers*, Phys. Rev. Lett. **117**, 187401 (2016).

[19] Z. Ye, D. Sun, and T. F. Heinz, *Optical Manipulation of Valley Pseudospin*, Nat. Phys. **13**, 26 (2017).

[20] B. W. H. Baugher, H. O. H. Churchill, Y. Yang, and P. Jarillo-Herrero, *Optoelectronic Devices Based on Electrically Tunable p-n Diodes in a Monolayer Dichalcogenide*, Nat. Nanotechnol. **9**, 262 (2014).

[21] J. R. Schaibley, H. Yu, G. Clark, P. Rivera, J. S. Ross, K. L. Seyler, W. Yao, and X. Xu, *Valleytronics in 2D Materials*, Nat. Rev. Mater. **1**, 16055 (2016).

[22] Z. Bomzon, G. Biener, V. Kleiner, and E. Hasman, *Space-Variant Pancharatnam-Berry Phase Optical Elements with Computer-Generated Subwavelength Gratings*, Opt. Lett. **27**, 1141 (2002).

[23] A. V. Kildishev, A. Boltasseva, and V. M. Shalaev, *Planar Photonics with Metasurfaces*, Science **339**, 1232009 (2013).

[24] N. Yu and F. Capasso, *Flat Optics with Designer Metasurfaces*, Nat. Mater. **13**, 139 (2014).

[25] G. S. Agarwal, *Anisotropic Vacuum-Induced Interference in Decay Channels*, Phys. Rev. Lett. **84**, 5500 (2000).

[26] P. K. Jha, N. Shitrit, J. Kim, X. Ren, Y. Wang, and X. Zhang, *Metasurface-Mediated Quantum Entanglement*, ACS Photonics **5**, 971 (2018).

[27] S. Pancharatnam, *Generalized Theory of Interference, and Its Applications*, Proc. Indian Acad. Sci. A **44**, 247 (1956).

[28] M. V. Berry, *The Adiabatic Phase and Pancharatnam's Phase for Polarized Light*, J. Mod. Opt. **34**, 1401 (1987).

[29] E. Hasman, Z. Bomzon, A. Niv, G. Biener, and V. Kleiner, *Polarization Beam-Splitters and Optical Switches Based on Space-Variant Computer-Generated Subwavelength Quasi-Periodic Structures*, Opt. Commun. **209**, 45 (2002).

[30] N. Shitrit, I. Bretner, Y. Gorodetski, V. Kleiner, and E. Hasman, *Optical Spin Hall Effects in Plasmonic Chains*, Nano Lett. **11**, 2038 (2011).

[31] D. Lin, P. Fan, E. Hasman, and M. L. Brongersma, *Dielectric Gradient Metasurface Optical Elements*, Science **345**, 298 (2014).

[32] G. Zheng, H. Mühlenbernd, M. Kenney, G. Li, T. Zentgraf, and S. Zhang, *Metasurface Holograms Reaching 80% Efficiency*, Nat. Nanotechnol. **10**, 308 (2015).

[33] M. Khorasaninejad, W. T. Chen, R. C. Devlin, J. Oh, A. Y. Zhu, and F. Capasso, *Metalenses at Visible Wavelengths: Diffraction-Limited Focusing and Subwavelength Resolution Imaging*, Science **352**, 1190 (2016).

[34] A. Pors, O. Albrektsen, I. P. Radko, and S. I. Bozhevolnyi, *Gap Plasmon-Based Metasurfaces for Total Control of Reflected Light*, Sci. Rep. **3**, 2155 (2013).

[35] E. Maguid, I. Yulevich, D. Veksler, V. Kleiner, M. L. Brongersma, and E. Hasman, *Photonic Spin-Controlled Multifunctional Shared-Aperture Antenna Array*, Science **352**, 1202 (2016).

[36] See Supplemental Material for the metasurface design, wavelength- and distance-dependent responses of the metasurface-enabled anisotropic decay rate, effect of the metasurface size on the metasurface-enabled anisotropic decay rate, and vacuum field mediated parameters of the metasurface-TMDC system.

[37] E. Hasman, V. Kleiner, G. Biener, and A. Niv, *Polarization Dependent Focusing Lens by Use of Quantized Pancharatnam-Berry Phase Diffractive Optics*, Appl. Phys. Lett. **82**, 328 (2003).

[38] L. Novotny and B. Hecht, *Principles of Nano-Optics* (Cambridge University Press, Cambridge, 2006).

[39] J. von Neumann, *Mathematical Foundation of Quantum Mechanics* (Princeton University Press, Princeton, 1932).

[40] M. Amani, D.-H. Lien, D. Kiriya, J. Xiao, A. Azcatl, J. Noh, S. R. Madhvapathy, R. Addou, S. KC, M. Dubey *et al.*, *Near-Unity Photoluminescence Quantum Yield in MoS_2*, Science **350**, 1065 (2015).

[41] H. Kim, D.-H. Lien, M. Amani, J. W. Ager, and A. Javey, *Highly Stable Near-Unity Photoluminescence Yield in Monolayer MoS_2 by Fluoropolymer Encapsulation and Superacid Treatment*, ACS Nano **11**, 5179 (2017).

[42] G. S. Agarwal, *Quantum Statistical Theories of Spontaneous Emission and Their Relation to Other Approaches*, in Quantum Optics, Vol. 70 of Springer Tracts in Modern Physics (Springer-Verlag, Berlin, 1974).

[43] P. K. Jha, X. Ni, C. Wu, Y. Wang, and X. Zhang, *Metasurface-Enabled Remote Quantum Interference*, Phys. Rev. Lett. **115**, 025501 (2015).

[44] X. Ren, P. K. Jha, Y. Wang, and X. Zhang, *Nonconventional Metasurfaces: From Non-Hermitian Coupling, Quantum Interactions, to Skin Cloak*, Nanophotonics **7**, 1233 (2018).

[45] T. Stav, A. Faerman, E. Maguid, D. Oren, V. Kleiner, E. Hasman, and M. Segev, *Quantum Metamaterials: Entanglement of Spin and Orbital Angular Momentum of a Single Photon*, arXiv:1802.06374.

[46] K. Wang, J. G. Titchener, S. S. Kruk, L. Xu, H.-P. Chung, M. Parry, I. Kravchenko, Y.-H. Chen, A. S. Solntsev, Y. S. Kivshar *et al.*, *Quantum Metasurface for Multi-Photon Interference and State Reconstruction*, arXiv:1804.03494.

[47] Z. Li, Y. Li, T. Han, X. Wang, Y. Yu, B. Tay, Z. Liu, and Z. Fang, *Tailoring MoS_2 Exciton-Plasmon Interaction by Optical Spin-Orbit Coupling*, ACS Nano **11**, 1165 (2017).

[48] X. Lin, Y. Yang, N. Rivera, J. J. López, Y. Shen, I. Kaminer, H. Chen, B. Zhang, J. D. Joannopoulos, and M. Soljaĉić, *All-Angle Negative Refraction of Highly Squeezed Plasmon and Phonon Polaritons in Graphene-Boron Nitride Heterostructures*, Proc. Natl. Acad. Sci. USA **114**, 6717 (2017).

[49] L. Sun, C.-Y. Wang, A. Krasnok, J. Choi, J. Shi, J. S. Gomez-Diaz, A. Zepeda, S. Gwo, C.-K. Shih, A. Alù *et al.*, *Routing Valley Excitons in a Monolayer MoS_2 with a Metasurface*, arXiv:1801.06543.

[50] Y. Jiang, X. Lin, T. Low, B. Zhang, and H. Chen, *Group-Velocity-Controlled and Gate-Tunable Directional Excitation of Polaritons in Graphene-Boron Nitride Heterostructures*, Laser Photonics Rev. **12**, 1800049 (2018).

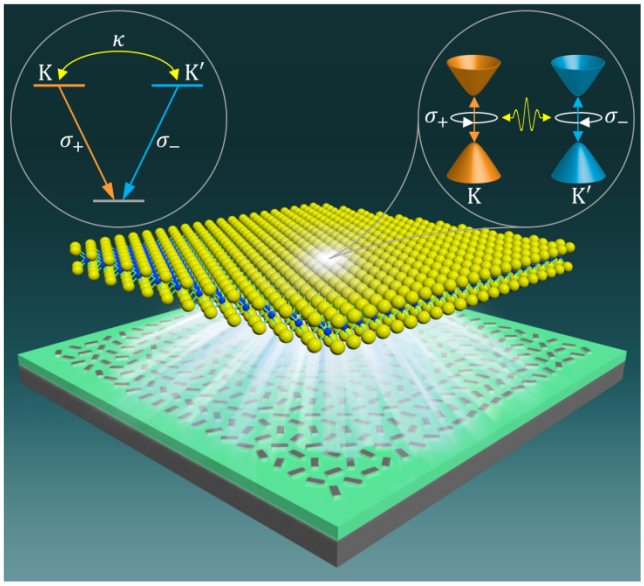

FIG. 1. Noise-induced valley coherence in transition metal dichalcogenide monolayers. We considered a monolayer of MX_2, positioned at a distant height from the metasurface. We designed a metasurface such that the spontaneous emission from the locally excited TMDC monolayer is efficiently focused back towards the source at the single photon level. Moreover, we engineered the polarization-dependent response of the metasurface to achieve an anisotropic scattered field. The interaction between the suspended TMDC monolayer and the custom-designed metasurface yields an anisotropic quantum vacuum. In an ordinary vacuum such as free space, the emission from K valley with σ_+ polarization cannot radiatively excite the orthogonal K′ valley with σ_- polarization. However, by breaking the isotropic nature of the quantum vacuum in the vicinity of the monolayer via a metasurface, one can remarkably excite K′ valley with an emission from K valley. Such interaction leads to spontaneous generation of valley coherence and yields quantum interference among their emissions.

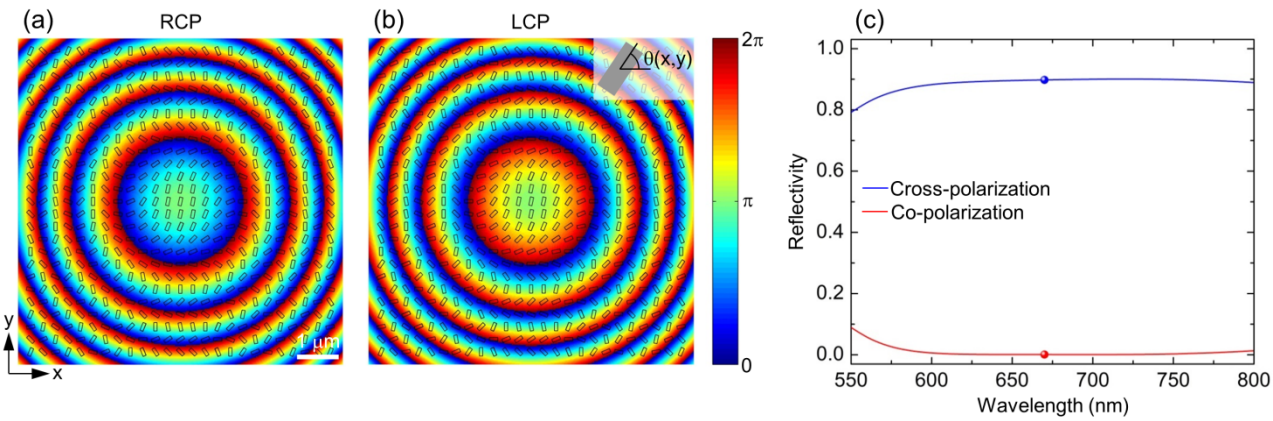

FIG. 2. Geometric phase-based metasurface for an anisotropic quantum vacuum. (a),(b) Phase profiles for molding the incident light with right circular polarization (RCP) and left circular polarization (LCP), respectively, at a free-space wavelength of $\lambda = 670$ nm and a height of the dipole from the metasurface of $d = 10\lambda$. The polarization helicity-dependent phase profiles are presented by the heat map and the corresponding metasurface realization, i.e., a nanorod antenna array with space-variant orientations $\theta(x,y)$, is shown on top. The width (x dimension) and length (y dimension) of each nanorod are 200 nm and 80 nm, respectively, and the thickness is 30 nm. The individual antenna design relies on a gap plasmon resonator nanoantenna with a 30-nm-thick silver nanorod, a 110-nm-thick dielectric (MgF_2) spacer layer, and a 130-nm-thick silver layer acting as a back reflector. We used a set of 16 nanoantenna orientations mimicking phase shifters with a $\pi/8$ phase increment. (c) Wavelength-dependent reflection efficiency of the GPM. By optimizing the dimensions of the nanorod, we achieved a broadband high cross-polarization reflectivity (90%) and an extremely low co-polarization reflectivity (~0.1%), yielding a highly efficient GPM. The dots highlight the reflectivities at 670 nm, which is the resonant wavelength for MoS_2 monolayer.

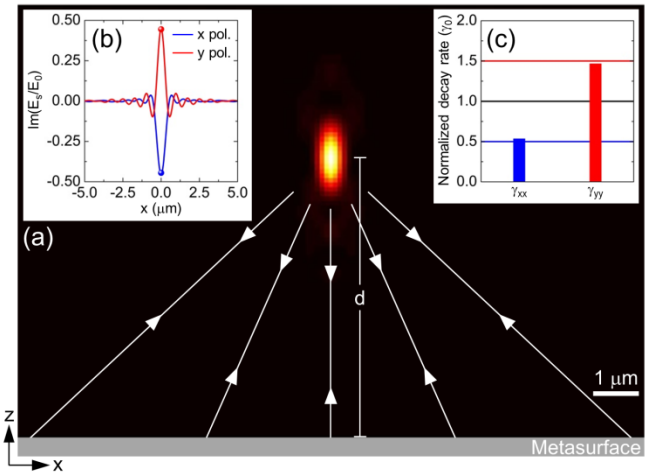

FIG. 3. Metasurface-induced an anisotropic decay rate. (a) Simulated scattered field intensity ($|E_x|^2$) distribution for the excitonic-dipole source located at $(0,0,10\lambda)$ and oriented along the x axis. The distribution is shown in the x-z plane, where the metasurface lies in $z = 0$ plane. With an optimized design, we achieved that ~47% reflection of the incident field focused back towards the on-demand location of the dipole (50% is the upper limit). The scattered field intensity ($|E_y|^2$) distribution for a y-polarized dipole is identical. (b) Nondegenerate imaginary part of the scattered field. At the position of the dipole (i.e., $x = 0$), for x- and y-polarized dipoles, the imaginary part of the scattered field is π-phase shifted, i.e., minimized for a x-polarized dipole while symmetrically maximized for a y-polarized dipole. The upper limit for the scattered field is E_0, which is the imaginary part of the field induced by the dipole at its position. (c) An anisotropic decay rate is enabled by the GPM, where the normalized decay rate for x- (γ_{xx}) and y-polarized dipoles (γ_{yy}) is suppressed (0.53) and symmetrically enhanced (1.47), respectively.

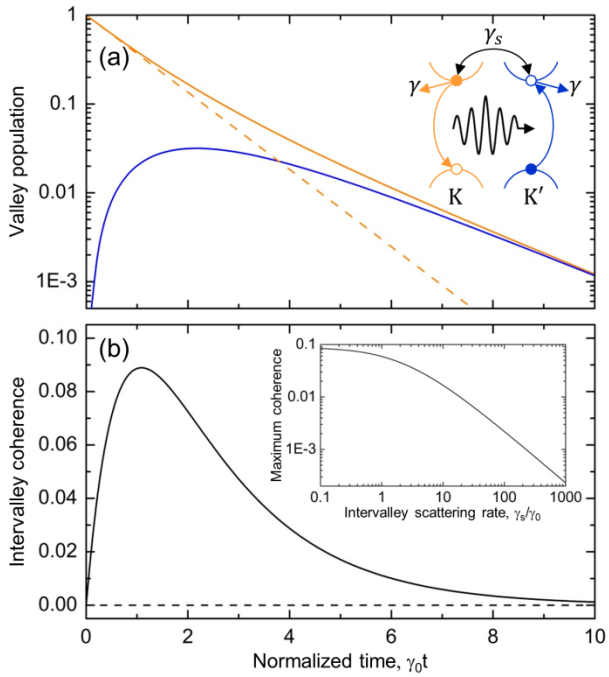

FIG. 4. Noise-induced valley population-coherence coupling. (a) Temporal evolution of the population of mutually orthogonal valleys (K and K′) in the presence (solid lines) and absence (dashed line) of the metasurface. In the presence of the metasurface, the decay rate of K valley population is reduced along with a finite excitation of the K′ valley. (b) Temporal evolution of intervalley coherence. A nonzero intervalley coherence, indicating coherent excitation of K′ valley with a photon emitted from K valley, is evident. This excitation is forbidden in free space (dashed line) due to an optical selection rule. The inset shows the dependence of the maximum intervalley coherence on the intervalley scattering rate, revealing that the generated coherence survives even when the intervalley scattering rate is 1000-fold stronger than the spontaneous decay rate.